HR-μMAS NMR-based metabolomics: localized metabolic profiling of a garlic clove with μg tissues

Covadonga Lucas-Torres, Gaspard Huber, Atsuyuki Ichikawa, Yusuke Nishiyama, Alan Wong

HR-µMAS NMR-based metabolomics: localized metabolic profiling of a garlic clove with µg tissues

Covadonga Lucas-Torres,[a] Gaspard Huber,[a] Atsuyuki Ichikawa,[b] Yusuke Nishiyama,[b,c] Alan Wong[a,*]

a) *NIMBE, CEA, CNRS, Université Paris-Saclay, CEA Saclay 91191 Gif-sur-Yvette, France*

b) *JEOL RESONANCE Inc., Musashino, Akishima, Tokyo 196-8558, Japan*

c) *RIKEN-JEOL Collaboration Center, Yokohama, Kanagawa 230-0045, Japan*

Contact: alan.wong@cea.fr (AW)

Keywords: HR-μMAS NMR, localized metabolic profiling, multivariate analysis, quantification, garlic *Allium sativum*

ABSTRACT: The localization of metabolic profiles within a tissue sample is of particular interest when the sampling size is considerably small, i.e. in the order of microgram (µg) scale. Small sampling size is inevitable when the sample availability is limited, or when different metabolic profiles are suspected in small disparate sample regions. Capitalizing a recently introduced high-resolution micro-MAS probe (HR-µMAS) for its capability of high-quality NMR data acquisition of µg samples, this study explores the localized metabolic NMR profiling of a single garlic clove and compares the methodology and results with the standard HR-MAS. One advantage of HR-µMAS is the feasibility of analyzing homogenous µg samples within a large heterogeneous tissue. As a result, the sampling mass (< 0.5 mg) allows to selectively profile four homogenous anatomic garlic regions by HR-µMAS (skin, flesh, inner epidermis and sprout), in contrast to three regions (skin, flesh and core ≡ inner epidermis & sprout) by HR-MAS with a sampling mass of ca. 8 mg. Discriminant analysis was carried out to identify the significant variables in the different regions. It found a significant presence of fructose in both skin and flesh, while sucrose and glucose are predominant in the core. Among the garlic characteristic sulfur compounds, allicin is dominant in the core and allyl mercaptan in both skin and flesh. Quantification analysis was conducted and demonstrated its potential by quantifying metabolites at µg-level. This study offers an important basis for designing HR-µMAS NMR-based metabolomics studies that can benefit from profiling µg-scale samples.

INTRODUCTION

Metabolomics comprises a set of analytical protocols for the identification, characterization and quantification of small molecules (metabolites) that are the result of biochemical processes in a specimen (e.g. tissue) of interest. The accurate obtainment and correct interpretation of the metabolic profiles from samples require dedicated techniques. For example, obtaining spatially localized metabolic constituents within a specimen can be beneficial for data analysis and interpretation. One commonly used spectroscopic technique is the localized magnetic resonance spectroscopy (MRS) – it is essentially an *in vivo* spectroscopic method of nuclear magnetic resonance (NMR) applied in magnetic resonance imaging (MRI). MRS has found success in brain research for identifying the local metabolic activities.[1-3] However, one limitation in MRS is the lack of high spectral resolution for deducing a comprehensive metabolic profile.[4] For this reason, MRS is seldom applied in food research.[5,6] On the contrary, the advance of mass spectrometry imaging (MSI) has now become a valuable profiling tool in food science,[7,8] that allows localizing molecules with specific molecular weights.

High-resolution magic angle spinning (HR-MAS) has proven to be a useful analytical tool for a wide range of morphology in diseased samples, such as the solid-like amyloidogenic proteins in Alzheimer[9] and the semi-solid in tumorous tissues.[10,11] Moreover, HR-MAS has also been exploited in food tissues.[12-14] The high spectral resolution from HR-MAS enables to provide a comprehensive localized metabolic profiling of a large specimen. It can be carried out by systematically sampling

region-by-region of a specimen such as a renal cortex[15] of a rat kidney and a rat brain,[16] and on vegetables.[17,18]

However, in some cases, the large sampling volume (in mm^3) by HR-MAS might not be sufficient for small-scale specimens. Indeed, small volume (in μm^3) will facilitate the sample obtainment, although it impairs on the NMR sensitivity. To overcome this issue, Wong *et al*. have recently introduced a high-resolution capable micro-sized MAS probe technology (denoted as HR-μMAS) targeting metabolomic applications of μg-scale sampling.[19,20] However, HR-μMAS has yet to be demonstrated on a metabolomics designated protocol, from data collection to multivariate data analysis. This study performs an *ex-situ* localized NMR metabolic profiling with HR-μMAS on a single garlic clove tissue (*Allium sativum*) and it is designed to examine the HR-μMAS application to metabolomics.

Despite there are numerous studies on the phytochemical compositions of garlic,[21,22] there is only one report on localized profiling and it was carried out by mass spectrometry imaging.[23] In this study, garlic clove is strategically chosen because of the distinct anatomic regions – skin for protection, flesh for energy storage and core for sprouting including a thin protective layer of inner epidermis[24] – which already suggest the different phytochemical makeup in each region.

EXPERIMENTAL SECTION

Sample preparation

(a) Phenylalanine solution. 90 and 120 mM of phenylalanine (Phe) were prepared in D_2O (0.05 wt% TSP, i.e. 3-(trimethylsilyl)-propionic-2,2,3,3-d_4 acid sodium salt), and stored at 4 °C until analysis.

(b) Garlic clove tissue. Bulbs of French raw purple garlic were collected locally. Cloves were peeled and cut transversely in bulk pieces revealing the distinct regions (shown in Fig. S-1 in supporting information (SI): skin (S), flesh (F) and core (C), in which it consists of the sprout (Sp) at the centre surrounded by the inner epidermis (IE)). For HR-MAS, a 2-mm biopsy punch was used to extract the specific tissue (S, F and C) with n = 6. The tissues were then introduced into a Kel-F bioinsert together with 8 μL of D_2O (0.05 wt% TSP). The mean D_2O content in the samples was about 45 wt%. The preparation was restricted to <5 min to avoid sample degradation. For HR-μMAS, a 0.5-mm biopsy punch was used to extract the tissue (with n = 6 for S, F and IE; and n = 8 for Sp) and to inject it directly into the 1-mm rotor. D_2O (0.05 wt% TSP) was pipetted into the rotor and followed by enclosing with a rotor cap. The mean D_2O content was about 32 wt%. The entire procedure was performed under an Olympus stereoscope and was restricted to <15 min. All sampling masses in HR-MAS and HR-μMAS were determined by the weight difference.

MAS NMR experiments. ^1H NMR experiments were carried out on a Bruker Avance II operating at a ^1H frequency of 499.16 MHz with a 4-mm HR-MAS or a custom-built 1-mm HR-μMAS under a sample spinning at 4000 ± 2 Hz (for HR-MAS) and ± 100 Hz (for HR-μMAS), at a constant temperature of 20 ± 2 °C. Carr-Purcell-Meiboom-Gill (CPMG) was used acquiring spectral data of the garlic tissue, with a

1 s water suppression and an echo period of 16 ms. For quantifiable spectra, a 16.7 s recycle-delay followed by a 1 s low-power water suppression was used in the CPMG experiment. The ^{1}H chemical shift was referenced to the alanine doublet at 1.48 ppm. The spectral processing was performed using Bruker Topspin 3.5 with a line broadening of 0.3 Hz applied prior to Fourier transform.

Data analysis

(a) Multivariate data analysis. The processed spectral data were uploaded into MestreNova v8.1. The spectra (8.7 to -0.05 ppm) were aligned, and the HDO region was removed between 4.66 and 5.05 ppm using a blind region function. Each spectrum was divided into sub-ppm buckets: 0.015 ppm for the phenylalanine solutions data and 0.02 ppm for the garlic data. The signal area under each bucket was integrated and normalized to a constant sum of all integrals. The normalized data of the garlic was subsequently corrected using the PQN (probabilistic quotient normalization)[25] due to the variations in sampling mass. The data matrix was exported to SIMCA P13 to proceed with the multivariate modelling. It was scaled using the Pareto scaling. Unsupervised PCA was performed, followed by supervised OPLS-DA analysis. The models were validated by assessing the values of R^2X, R^2Y and Q^2, as well as by the p-values obtained from cross-validation (level of confidence <0.05) to avoid over-fitting.

(b) Quantification. The spectra were submitted to peak integration using MestreNova v8.1. The absolute integral areas of the identified signals were used together with the absolute integral area of TSP to calculate the concentrations (the detail can be found in SI).

RESULTS AND DISCUSSION

Assessments on HR-μMAS

(a) Resolution and sensitivity. Fig. 1a displays a spectrum of Phe 90 mM showcasing the high-quality data acquired with HR-μMAS. The spectral resolution (with a full-width at half maximum (FWHM) of 0.03 ± 0.01 ppm for -CH at 3.99 ppm) is on-par to those obtained from standard NMRs, 0.03 ± 0.01 ppm for both HR-MAS and liquid probes. The J-splitting depth (i.e. the height ratio of the splitting and the signal) is also a good indicator and is found to be 73% for HR-μMAS and 77% and 69% for HR-MAS and liquid probes, respectively. The spectral resolution – in conjunction with a miniature coil – enhances the detection sensitivity, which can be evaluated by the limits of detection (LOD) and quantification (LOQ). The LOD and LOQ of HR-μMAS for phenylalanine are 0.29 ± 0.02 nmol/√min and 0.97 ± 0.04 nmol/√min, respectively. These values are found to be lower compared to those observed using HR-MAS or liquid NMR probes (Table 1). Aside from numerical indicators, the spectrum in Fig. 1a also displays its sensitivity to μmol detection in a microliter volume sample. This can be exemplified by the impurity ethanol signals (the triplet at 1.19 and quartet at 3.66 ppm). Based on the internal TSP reference (i.e. equation E-1 in SI), the ethanol concentration is found to be 0.93 ± 0.12 mM (i.e. 0.46 nmol in 490 nL) and is akin to the metabolic-level.[11]

(b) Quantitative NMR. Metabolic quantification requires high spectral resolution and sensitivity (i.e. LOQ) for accuracy and reliable data repeatability. As shown in Fig. 1b, the quantified concentrations – by equation E-1 – from HR-μMAS are similar to those from the standard NMRs. All measured concentrations are about 4-8 % below

the expected values. The variation among the 10-sampling data of HR-μMAS is minimal with standard deviations SD_{120mM} = 1.15 mM, SD_{90mM} = 0.53 mM, on-par with the standard NMRs: HR-MAS SD_{120mM} = 0.45 mM, SD_{90mM} = 0.47 mM; and liquid SD_{120mM} = 0.20 mM, SD_{90mM} = 0.14 mM. The good repeatability of the 10-sampling is also attested by the unsupervised multivariate PCA analysis using the spectral area between 0.05–8.7 ppm (Fig. 1c). It shows a single component (PC1) differentiating the data set according to the concentrations with insignificant data variation.

Localized profiling of a garlic clove. Localized metabolic HR-μMAS NMR profiling of a garlic clove tissue is performed here to discriminate the significant metabolites among the visible anatomical regions (Fig. S-1a): clove skin (S), flesh (F), inner epidermis (IE) and sprout (Sp). The results are compared to those by HR-MAS for assessing the HR-μMAS methodology as an NMR technique applicable to metabolomics.

(a) Tissue sampling size. For simplicity, a biopsy punch is used for extracting the garlic tissue and displacing it directly into the rotor. The thickness of S and IE is smaller than 2 mm, contrary to F and Sp; thus, it is inevitable extracting heterogeneous tissue (mixing two regions, as shown Fig. S-1a) with a 2-mm diameter punch chosen for the HR-MAS profiling (sampling mass ca. 8 ± 1 mg). On the other hand, a significantly smaller diameter 0.5-mm punch (sampling mass <0.5 mg) is used for HR-μMAS, increasing the likeliness of extracting homogenous tissues. As a result, HR-MAS is only capable of sampling three garlic regions (S,

F and C ≡ IE + Sp), whereas HR-μMAS can sample all four distinct regions (S, F, IE and Sp).

(b) NMR spectral comparison. The representative spectra of ^{1}H HR-MAS and HR-μMAS are shown in Fig. 2. Despite the similar acquisition time 15 min – but ca. 10-fold less in sampling-mass for HR-μMAS – the SNRs (measured from the allicin signal at 5.98 ppm) from both experiments are of the same order, with 76 in HR-MAS and 44 in HR-μMAS. The expanded spectra reveal slightly lower in spectral resolution for HR-μMAS with a FWHM 0.03 ± 0.01 ppm and a J-splitting depth 78 %, as compared to 0.03 ± 0.01 ppm and 86 % for HR-MAS.

In general, ^{1}H HR-MAS and HR-μMAS spectra are dominated by the intense signals of the carbohydrates – mainly fructose and sucrose – between 3.5–4.5 ppm. It makes up of 70–80 % of the total spectral intensity. Spectra also exhibit weak resonances in the aromatic region (7–8 ppm), shown in Fig. S-2. Distinct sets of multiplets between 5 and 6 ppm are also found in Fig. 2, which are associated with the organosulfur compounds responsible for the garlic aroma. In particular, the multiplets at 5.98 and 5.83 ppm are respectively assigned to allicin (2-propene-1-sulfinothioic acid S-2-propenyl ester) and its metabolized compound allyl mercaptan (2-propene-1-thiol), respectively. A complete and a comparative list of the NMR assignments in HR-MAS and HR-μMAS spectra are summarized in Table S-1 in SI.

Despite the HR-MAS spectral profile of C in Fig. 2a being similar to that of the summation HR-μMAS spectrum of IE and Sp (Fig. S-3), the individual profiles exhibit a few variations between Sp and IE. For example, among the amino acids, the

signals of asparagine (2.86 ppm), glutamine (2.14 ppm) (Fig. 2b) and tryptophan (7.54 ppm) are found higher in IE (Fig. S-2). For carbohydrates, the β-glucose doublet (4.65 ppm) is observed solely in Sp (Fig. 2b). It is noteworthy that the strong presence of the fatty acid (FA) signals (i.e. 1.32 ppm) in Sp renders the main discrepancy between the summation HR-μMAS spectrum and the HR-MAS spectrum. The presence of fatty acids in Sp have also been observed by MSI.[23] The observed spectral difference could be attributed to the different sample preparation between HR-MAS and HR-μMAS, i.e. the D_2O content. The former contains 45 wt% of D_2O and the latter accounts of 32 wt%. For comparison, the summation HR-μMAS spectrum Sp+IE (Fig. S-3) is a near analogous to the HR-MAS spectrum of C with 35 wt% D_2O. Fig. S-4 shows the effect of different D_2O content on the resultant HR-MAS spectra. It reveals that increasing the D_2O content improves the resolution and increases I_{met}/I_{FA}. Aside from the resolution, one plausible explanation might be due to the variations in the spin relaxation of the metabolite and fatty acids signals in the different medium conditions. This might have explained the fact that the signals of fatty acids in the HR-μMAS model study (with 32 wt% D_2O) are higher than those in the HR-MAS model (with 45 wt% D_2O). The result in Fig. S-4 suggests the importance of the sample medium in NMR profiling.

(c) Multivariate analysis. Fig. 3a and 3b show the overview of the localized NMR data that can be discerned by an unsupervised PCA. The PCA of HR-MAS reveals a prominent data differentiation along PC1 between C and S + F. A subtle but visible variation along PC2 can also be found between S and F. The data set of

C displays a highly dispersed profile along PC2. One plausible explanation could be the sample heterogeneity in C, which is composed of Sp + IE. For HR-μMAS, the overall data distribution is a near analogous to that for HR-MAS: a separation along PC1 between S + F and Sp + IE which corresponds to C. No variation is observed between S and F by HR-μMAS. However, a discrete discrepancy is evident between Sp and IE along PC2.

S+F vs C (Sp+IE). Supervised discriminant analysis, OPLS-DA, is carried out to diagnose the latent metabolic variations that have led to the observed discrete patterns in PCA. Two groups of data are submitted to OPLS-DA: S+F and C (or Sp+IE). The S-line plots (Fig. 3c and 3e) generated from the OPLS-DA model exhibit NMR-like spectra with signals positioning on the chemical shift and with positive p[ctr] scores (covariance) associated to metabolites from S+F, and negative scores to those from C (or Sp+IE). As expected – since C is composed of Sp+IE – the profile of the S-line plot of the HR-μMAS model is analogous to that of the HR-MAS except with different degree of correlation coefficients p[corr]. For unambiguously identifying the significant variants in the region, additional score VIP (variable importance in the projection) is computed from the OPLS model to assist in identifying the variant metabolites between the groups. VIP is plotted as a function of p[corr] (Fig. 3d and 3f). The high significant variables with a high reliability in the model ($|p[corr]| > 0.75$) and a high importance ($VIP \geq 1$) are situated inside the red zone of the plot; the green zone represents those with moderate significance ($\pm 0.6 < |p[corr]| < 0.75$ and $VIP \geq 1$); and the marginal significances ($|p[corr]| > 0.75$ and $VIP \leq 1$) are displaced in the orange zone. By this scheme, a total of 24

metabolites are identified in the HR-MAS model and 18 in HR-μMAS (Table 2). Not all ascertained metabolites in the HR-MAS model are found in HR-μMAS, this is attributed to the fact that spectral quality of HR-μMAS is slight inferior to that of HR-MAS; however, improvement could be made with increased data averaging (i.e. instead of 15 min data acquisition, 4×15 min would double the sensitivity). Nonetheless, the overall identified variances by HR-μMAS and HR-MAS are in agreement with those found in a previous profiling study by mass spectroscopy imaging (MSI).[23] In general, the amino acids glutamine, leucine, asparagine and tryptophan are found in C. Whereas, arginine and phenylalanine are distributed throughout S+F. Arginine has previously reported as one of the major amino acids in garlic[26] with a storage function. It has also been suggested that phenylalanine has a storage function while tyrosine is distributed in the sprout[23] which is in agreement with the significance observed. Glutamate is metabolized into glutamine, and *vice versa* in plants.[27] This mechanism requires the plant root to absorb organic nitrogen sources from the soil, explaining the significance of glutamine in C. Similarly, asparagine is significant in C because it involves in the plant growth and accumulates in the sprout as a source of nitrogen.[28] The presence of tryptophan in C has also been previously found in the extracts of garlic sprouts.[29]

For organosulfur compounds, a marginal significance of allyl mercaptan is found in S+F, while its precursor, allicin, is relevant in C with high significance. This is attributed to the degradation of alliin (S-allyl-L-cysteine sulfoxide) to allicin,[24] whose mechanism can be triggered when the garlic clove is cut and exposed to air. However, allicin is an unstable compound[30] and decomposes into several allyl

sulfides including allyl mercaptan.[31] Conversely, the presence of allicin in C might have suggested that the inner region of garlic is protected against its degradation. The same observation has also been reported by MSI.[23]

A marginal significance of hydroxycinnamic acids is present in C. This is of particular interest because they are associated with the structural polymers of the vegetable cell walls. One of their main components is lignin. It is a robust macromolecule that provides protection and rigidity to the material, and it is composed of aromatic alcohol units.[32] The observation of metabolites with similar molecular structure, hydroxycinnamic acids, might suggest the presence of free lignin units,[33] in this case in C. This is consistent with the solid-state NMR data of the polymeric matter from the core region which is found containing lignin (detailed discussion in SI, Fig. S-5).

It is interesting to note that the NMR data –not in MSI[23] – also reveal a variation in carbohydrates. For example, fructose dominates in S+F, while sucrose does in C (Fig. 3). According to a previous study,[34] fructosan is the main polymer in vegetables, while sucrose and glucose are related to the growth of the sprout.

Sp vs IE. Capitalizing the localized data of Sp and IE obtained by HR-μMAS, OPLS-DA has been carried out, and 14 variant metabolites have been identified (Table 2). Fig. 4a shows the resultant S-line plot with positive p[ctr] scores associated with IE and negative to Sp. The amino acid glutamine has a moderate significance in IE, indicating that the significance of glutamine found in C in HR-MAS is due primarily to IE. The same observation can be found with asparagine.

The VIP-p[corr] plot (Fig. 4b) has identified the carbohydrate variants between Sp and IE. Fructose and glucose with high and moderate significant level, respectively, are found in IE. Moreover, the presence of hydroxycinnamic acids is also found predominantly in IE.

Among organosulfur compounds, cycloalliin (1.51 ppm) – a derivative of the gamma-glutamil peptides in garlic[35] – is discerned in HR-μMAS model with a moderate significance in IE of the core; however, cycloalliin is not classified as a significant variant in the HR-MAS model. This is because the samples used in HR-μMAS analysis have a higher degree of homogeneity than those in HR-MAS, rendering a higher sensitivity (i.e. simplified spectral data) for identifying the variants with low metabolic content, in this case, less than 150 μmol/g of cycloalliin (more discussion below). On the contrary, in HR-MAS analysis such variant is readily masked by the overcrowded data from a heterogeneous sample (mixing of Sp and IE). Similarly, methanol with 108 μmol/g is identified as a variant in IE with a moderate significance in the HR-μMAS model; but not in HR-MAS. In the case of amino acids, alanine (125 μmol/g), leucine, and arginine are found with high significance in Sp but are not considered as significant in the HR-MAS model. The capability of determining the metabolic variance with low concentrations illustrates the advantage of analysis by sampling microscopic quantity with an enhanced sample homogeneity.

(d) Quantitative analysis: Sp vs IE. Exploiting the quantifiable spectra (with long relaxation delay) acquired by HR-μMAS, a few metabolites with well-resolved signals are quantified (μmol/g) using equations E-2 and E-3 in SI. The results are summarized in Table 3. It should be emphasized that these values can only be

considered as estimations. Indeed, improving spectral quality could enhance its reliability and increase the number of quantifiable metabolites.

The highest content of the quantified metabolites is found to be glutamine with 1016 ± 171 μmol/g (n = 6) in IE, which is in agreement to the previous results reported.[36] According to the p-value (0.000167) by a student's t-test, there are significant differences between IE and Sp.

The quantified carbohydrates reveals a higher content of fructose (873 ± 171 μmol/g, n = 6) in IE as compared to Sp, with a p-value of 0.00177. A previous study[37] has found that fructosan is the main polysaccharide in an entire garlic bulb; but, no localized sugar composition was provided.

Based on the spectral profile, two sets of doublets are found in Sp (1.47 and 1.50 ppm) while only a single doublet at 1.50 ppm is observed in IE. The doublet at 1.50 ppm corresponds to cycloalliin[21] with relatively low concentrations, 68 ± 33 μmol/g in Sp and 146 ± 31 μmol/g in IE with a p-value of 0.00184. This is in agreement with the S-line plot in Fig. 4, which indicates a moderate significance of cycloalliin in IE with a |p[corr]| score of 0.665.

CONCLUSIONS. This study has assessed a new NMR probe technology, high-resolution micro-sized MAS (HR-μMAS probe), for metabolomics applications with a modest labour cost (i.e. 15 minutes for sample-preparation). The study provides an essential basis for NMR-based metabolic profiling using HR-μMAS. The quantitative NMR experiments (with Phe solution) have demonstrated an excellent spectral quality and data repeatability, comparable with standard NMRs (HR-MAS and

standard liquid NMR). Moreover, ^{1}H HR-μMAS NMR spectroscopy has been explored and evaluated for mapping the localized metabolic profiles in different anatomical regions of a garlic clove – S, F and C, and the latter contains a small region of Sp surrounded by a thin layer of IE. The data reliability has been assessed by the comparison with HR-MAS experiments. The combination of localized NMR sampling with the multivariate analysis provides a reliable tool to profile the metabolites with high significance for the discrimination between the garlic anatomic regions. In these sense, the obtainment of samples with high homogeneity is a crucial step: the small spatial resolution provided by HR-μMAS allows extracting adjacent anatomical samples within the whole tissue, thus, rendering the data analysis with an improved reliability of the model for offering information on its global heterogeneity. Further multivariate analysis within the two regions constituting the core (Sp and IE) that were not available in the HR-MAS model shows the utility of HR-μMAS application for providing with detailed localized information on a smaller sample volume.

Despite a food system is exploited in this demonstrative study, it provides an important basis of HR-μMAS NMR-based metabolomics to a wide range of biosystems, especially samples with low availability or with diverse anatomical regions. For example, the metabolic morphology of diseased tissues is of interest. HR-μMAS NMR could enhance the recognition of the growth patterns by the metabolic signatures and be used as a diagnostic tool. In the case of solid-like samples such as amyloidogenic proteins, this could benefit from HR-μMAS with fast sample spinning for offering high quality spectral data to deduce complex protein structures.

ACKNOWLEDGEMENTS

We would like to thank the French Agence Nationale de la Recherche (ANR) for the financial support under ANR-12-JSV5-0005 (HRMACS) and ANR-16-CE11-0023 (HRmicroMAS).

NOTE: The authors declare no competing financial interest

Supporting Information includes: NMR quantification procedure, a photo of a garlic clove, localized NMR spectra between 6.2-8.2 ppm, the spectral comparison between HR-µMAS and HR-MAS, medium effect on the HR-MAS spectra, and solid-state NMR of garlic; and a table of the peak assignments in HR-µMAS and HR-MAS.

REFERENCES

(1) Soares, D. P.; Law, M. Magnetic Resonance Spectroscopy of the Brain: Review of Metabolites and Clinical Applications. *Clin. Radiol.* **2009**, *64* (1), 12–21.

(2) Faghihi, R.; Zeinali-Rafsanjani, B.; Mosleh-Shirazi, M. A.; Saeedi-Moghadam, M.; Lotfi, M.; Jalli, R.; Iravani, V. Magnetic Resonance Spectroscopy and Its Clinical Applications: A Review. *J. Med. Imaging Radiat. Sci.* **2017**, *48* (3), 233–253.

(3) Lv, X.; Dong, Z.; Li, J.; Zhang, R.; Xie, C.; Zhang, Z. Brain Proton Magnetic Resonance Spectroscopy : A Review of Main Metabolites and Its Clinical Applications in Gliomas. *Curr. Mol. Imaging* **2015**, *4* (2), 76–84.

(4) Fuss, T. L.; Cheng, L. L. Evaluation of Cancer Metabolomics Using Ex Vivo High Resolution Magic Angle Spinning (HRMAS) Magnetic Resonance Spectroscopy (MRS). *Metabolites* **2016**, *6* (1), 11.

(5) Foucat, L.; Ofstad, R.; Renou, J.-P. How Is the Fish Meat Affected by Technological Processes? In *Modern Magnetic Resonance*; Webb, G. A., Ed.; Springer, 2008; pp 967–971.

(6) Laurent, W.; Bonny, J. M.; Renou, J. P. Muscle Characterisation by NMR Imaging and Spectroscopic Techniques. *Food Chem.* **2000**, *69* (4), 419–426.

(7) Kadam, S. U.; Misra, N. N.; Zaima, N. Mass Spectrometry Based Chemical Imaging of Foods. *RSC Adv.* **2016**, *6* (40), 33537–33546.

(8) Handberg, E.; Chingin, K.; Wang, N.; Dai, X.; Chen, H. Mass Spectrometry Imaging for Visualizing Organic Analytes in Food. *Mass Spectrom. Rev.* **2015**, *34*, 641–658.

(9) Wang, J.; Yamamoto, T.; Bai, J.; Cox, S. J.; Korshavn, K. J.; Monette, M.; Ramamoorthy, A. Real-time monitoring of the aggregation of Alzheimer's amyloid-β via ^{1}H magic angle spinning NMR spectroscopy. *Chem. Commun.* **2018**, *54*, 2000–2003

(10) Schennetti, L.; Mucci, A.; Parenti, F.; Cagnoli, R.; Righi, V.; Tosi, M. R.; Tugnoli, V. HR-MAS NMR Spectroscopy in the Characterization of Human Tissues: Application to Healthy Gastric Mucosa. *Concepts Magn. Reson. Part*

A Bridg. Educ. Res. **2010**, *88* (12), 430–443.

(11) Martínez-Bisbal, M. C.; Monleon, D.; Assemat, O.; Piotto, M.; Piquer, J.; Llácer, J. L.; Celda, B. Determination of Metabolite Concentrations in Human Brain Tumour Biopsy Samples Using HR-MAS and ERETIC Measurements. *NMR Biomed.* **2009**, *22* (2), 199–206.

(12) Corsaro, C.; Mallamace, D.; Vasi, S.; Ferrantelli, V.; Dugo, G.; Cicero, N. ^{1}H HR-MAS NMR Spectroscopy and the Metabolite Determination of Typical Foods in Mediterranean Diet. *J. Anal. Methods Chem.* **2015**, *2015*, 1–14.

(13) Corsaro, C.; Cicero, N.; Mallamace, D.; Vasi, S.; Naccari, C.; Salvo, A.; Giofrè, S. V.; Dugo, G. HR-MAS and NMR towards Foodomics. *Food Res. Int.* **2016**, *89* (3), 1085–1094.

(14) Valentini, M.; Ritota, M.; Cafiero, C.; Cozzolino, S.; Leita, L.; Sequi, P. The HRMAS-NMR Tool in Foodstuff Characterisation. *Magn. Reson. Chem.* **2011**, *49*, S121-S125.

(15) Garrod, S.; Humpfer, E.; Spraul, M.; Connor, S. C.; Polley, S.; Connelly, J.; Lindon, J. C.; Nicholson, J. K.; Holmes, E. High-Resolution Magic Angle Spinning ^{1}H NMR Spectroscopic Studies on Intact Rat Renal Cortex and Medulla. *Magn. Reson. Med.* **1999**, *41* (6), 1108–1118

(16) Tsang, T. M.; Griffin, J. L.; Haselden, J.; Fish, C.; Holmes, E. Metabolic Characterization of Distinct Neuroanatomical Regions in Rats by Magic Angle Spinning ^{1}H Nuclear Magnetic Resonance Spectroscopy. *Magn. Reson. Med.* **2005**, *53* (5), 1018–1024.

(17) Pérez, E. M. S.; Iglesias, M. J.; Ortiz, F. L.; Pérez, I. S.; Galera, M. M. Study of the Suitability of HRMAS NMR for Metabolic Profiling of Tomatoes: Application to Tissue Differentiation and Fruit Ripening. *Food Chem.* **2010**, *122* (3), 877–887.

(18) Mucci, A.; Parenti, F.; Righi, V.; Schenetti, L. Citron and Lemon under the Lens of HR-MAS NMR Spectroscopy. *Food Chem.* **2013**, *141* (3), 3167–3176.

(19) Nishiyama, Y.; Endo, Y.; Nemoto, T.; Bouzier-Sore, A.-K.; Wong, A. High-Resolution NMR-Based Metabolic Detection of Microgram Biopsies Using a 1 mm HRμMAS Probe. *Analyst* **2015**, *140* (24), 8097–8100.

(20) Duong, N. T.; Endo, Y.; Nemoto, T.; Kato, H.; Bouzier-Sore, A.-K.; Nishiyama, Y.; Wong, A. Evaluation of a High-Resolution Micro-Sized Magic Angle Spinning (HRμMAS) Probe for NMR-Based Metabolomic Studies of Nanoliter Samples. *Anal. Methods* **2016**, *8* (37), 6815–6820.

(21) Liang, T.; Wei, F.; Lu, Y.; Kodani, Y.; Nakada, M.; Miyakawa, T.; Tanokura, M. Comprehensive NMR Analysis of Compositional Changes of Black Garlic during Thermal Processing. *J. Agric. Food Chem.* **2015**, *63* (2), 683–691.

(22) Ritota, M.; Casciani, L.; Han, B.-Z.; Cozzolino, S.; Leita, L.; Sequi, P.; Valentini, M. Traceability of Italian Garlic (Allium Sativum L.) by Means of HRMAS-NMR Spectroscopy and Multivariate Data Analysis. *Food Chem.* **2012**, *135* (2), 684–693.

(23) Misiorek, M.; Sekuła, J.; Ruman, T. Mass Spectrometry Imaging of Low Molecular Weight Compounds in Garlic (*Allium Sativum* L.) with Gold Nanoparticle Enhanced Target. *Phytochem. Anal.* **2017**, *28*, 479–486.

(24) Ellmore, G. S.; Feldberg, R. S. Allin Lyase Localization in Bundle Sheats of the Garlic Clove (Allium Sativum). *Am. J. Bot.* **1994**, *81* (1), 89–94.

(25) Dieterle, F.; Ross, A.; Schlotterbeck, G.; Senn, H. Probabilistic Quotient Normalization as Robust Method to Account for Dilution of Complex Biological Mixtures. Application In ^{1}H NMR Metabonomics. *Anal. Chem.* **2006**, *78* (13), 4281–4290.

(26) Lawson, L. D.; Gardner, C. D. Composition , Stability , and Bioavailability of Garlic Products Used in a Clinical Trial. *J. Agric. Food Chem.* **2005**, *53*, 6254–6261.

(27) Forde, B. G.; Lea, P. J. Glutamate in Plants: Metabolism, Regulation, and Signalling. *J. Exp. Bot.* **2007**, *58* (9), 2339–2358.

(28) Lea, P. J.; Sodek, L.; Parry, M. A. J.; Shewry, P. R.; Halford, N. G. Asparagine in Plants. *Ann. Appl. Biol.* **2007**, *150* (1), 1–26.

(29) Gdula-Argasińska, J.; Paśko, P.; Sułkowska-Ziaja, K.; Kała, K.; Muszyńska, B. Anti-Inflammatory Activities of Garlic Sprouts, a Source of α-Linolenic Acid and 5-Hydroxy-l-Tryptophan, in RAW 264.7 Cells. *Acta Biochim. Pol.* **2017**, *64* (3), 551–559.

(30) Borlinghaus, J.; Albrecht, F.; Gruhlke, M.; Nwachukwu, I.; Slusarenko, A. Allicin: Chemistry and Biological Properties. *Molecules* **2014**, *19* (8), 12591–12618.

(31) Rahman, K.; Lowe, G. M. Significance of Garlic and Its Constituents in Cancer and Cardiovascular Disease Garlic and Cardiovascular Disease : A Critical Review 1 , 2. *J. Nutr.* **2006**, *136* (2), 736–740.

(32) Foston, M.; Samuel, R.; He, J.; Ragauskas, A. J. A Review of Whole Cell Wall NMR by the Direct-Dissolution of Biomass. *Green Chem.* **2016**, *18* (3), 608–621.

(33) Kleinert, M.; Barth, T. Phenols from Lignin. *Chem. Eng. Technol.* **2008**, *31* (5), 736–745.

(34) Edelman, J.; Jefford, T. G. The Mechanisim of Fructosan Metabolism in Higher Plants As Exemplified in Helianthus Tuberosus. *New Phytol.* **1968**, *67* (3), 517–531.

(35) Ichikawa, M.; Ide, N.; Ono, K. Changes in Organosulfur Compounds in Garlic Cloves during Storage. *J. Agric. Food Chem.* **2006**, *54* (13), 4849–4854.

(36) Montaño, A.; Casado, F. J.; De Castro, A.; Sánchez, A. H.; Rejano, L. Vitamin Content and Amino Acid Composition of Pickled Garlic Processed with and without Fermentation. *J. Agric. Food Chem.* **2004**, *52* (24), 7324–7330.

(37) Mann, L. K. Anatomy of the Garlic Bulb and Factors Affecting Bulb Development. *Hilgardia* **1952**, *21*, 195–251.

Figure Captions

Figure 1 (a) A representative HR-μMAS ^{1}H NMR spectrum of Phe 90 mM (at 500 MHz). The chemical shift ranges between 3.0–3.4 and 3.9–4.1 ppm are expanded for clarity. Signals from the EtOH impurity are highlighted and quantified. (b) A bar plot with the measured concentrations of Phe solutions and their standard deviations of the three different NMR approaches (green = HR-μMAS, blue = HR-MAS, yellow = standard liquid). The expected concentration is plotted for comparative purposes (grey). (c) PCA score plot of acquired NMR data from HR-μMAS. Quality parameters: 1-component, $R^2X = 0.727$, $Q^2 = 0.69$.

Figure 2 Spectral comparison of the garlic regions between (a) HR-MAS and (b) HR-μMAS. The intensities are normalized to that of the sucrose signal at 5.42 ppm. The assigned metabolites are indicated. The chemical shift range between 5.3–6.0 ppm is amplified showcasing the spectral quality.

Figure 3 PCA score plots obtained for the separation of the garlic regions using the (a) HR-MAS spectral data and (b) HR-μMAS. The spectra data corresponding to skin (S), flesh (F) and core (C) for HR-MAS; and S, F, sprout (Sp) and inner epidermis (IE) for HR-μMAS, are clustered in specific colors for a better readability. Quality parameters: for HR-MAS, 3-components, $R^2X = 0.919$, $Q^2 = 0.843$; for HR-μMAS, 5-components, $R^2X = 0.934$, $Q^2 = 0.839$. The corresponding OPLS-DA were carried out to identify the latent variants. The S-line plots (c) HR-MAS and (e) HR-μMAS identify a few significant variables in S+F (p[ctr] **>** 0) and C (p[ctr] < 0) in HR-MAS, or Sp+IE (p[ctr] < 0) in HR-μMAS. The significant level p[corr] is indicated by a color scheme. The VIP-p[corr] plots (e) HR-MAS and (f) HR-μMAS facilitate the identification of a complete list of metabolic variants. Quality parameters of OPLS-DA: for HR-MAS, 1 predictive component and 1 orthogonal component, $R^2X = 0.888$, $R^2Y = 0.982$, $Q^2 = 0.968$, p-value (CV) = $7.61*10^{-9}$; and for HR-μMAS, 1 predictive component and 1 orthogonal component, $R^2X = 0.806$, $R^2Y = 0.975$, $Q^2 = 0.964$, p-value (CV) = $1.81*10^{-13}$.

Figure 4 (a) S-line plot and (b) VIP-p[corr] plot used to identify the significant variables responsible of variations between Sp and IE. Quality parameters of OPLS-DA: 1 predictive component and 2 orthogonal components, $R^2X = 0.747$, $R^2Y = 0.955$, $Q^2 = 0.828$, p-value (CV) = 0.027.

Table 1. Comparative values of the spectral quality of a 90 mM Phe.

Acq. method	Acq. time (min)	Conc. (mM)	Vol. (µl)	SNR[a]	FWHM (ppm)	Split depth (%)	LOD/√time (nmol/√min)	LOQ/√time (nmol/√min)
HR-µMAS (n=10)	12.46	87.09 ± 0.53	0.49	118.72 ± 6.53	0.03 ± 0.01	73	0.29 ± 0.02	0.97 ± 0.04
HR-MAS (n=3)	15.09	86.60 ± 0.47	16	697.34 ± 171.63	0.03 ± 0.01	77	1.51 ± 0.44	5.03 ± 1.46
Liquid (n=3)	0.47	87.15 ± 0.14	600	619.87 ± 22.77	0.03 ± 0.01	69	368.17 ± 13.77	1227.24 ± 45.91

a) acq. parameters of a single-pulse experiment: HR-µMAS number of scans=32, relaxation delay=20 s; HR-MAS number of scans=32, relaxation delay=25 s; standard liquid number of scans=1, relaxation delay=25 s.

Table 2. Significant metabolites for the discrimination from the HR-MAS and HR-μMAS models.

		HR-MAS model			HR-μMAS model		
S+F	**Variable (ppm)[d]**	**VIP**	**p[corr]**	**Significance[e]**	**VIP**	**p[corr]**	**Significance[e]**
arginine	1.75	1.526	-0.930	high	1.539	-0.971	high
pyroglutamate	2.53	0.982	-0.816	marginal	1.011	-0.835	high
threonine	4.29	1.308	-0.918	high	1.572	-0.904	high
phenylalanine	7.38	0.428	-0.949	marginal	0.419	-0.932	marginal
fructose	4.13	4.297	-0.987	high	4.119	-0.99	high
cystine	4.33	0.507	-0.753	marginal	0.751	-0.728	marginal
allyl mercaptan	5.18	0.879	-0.880	marginal	0.694	-0.874	marginal
Choline	3.17	0.471	-0.779	marginal	0.561	-0.838	marginal
UMP	8.12	0.385	-0.879	marginal	0.447	-0.82	marginal
C or Sp+IE[a]	**Variable (ppm)**	**VIP**	**p[corr]**	**Significance[e]**	**VIP**	**p[corr]**	**Significance[e]**
leucine	0.97	0.581	0.897	marginal	-	-	-
valine	1.03	0.338	0.838	marginal	0.482	0.813	marginal
lactate	1.37	1.185	0.921	high	-	-	-
proline	2.09	1.092	0.971	high	-	-	-
glutamine	2.47	1.865	0.857	high	1.594	0.781	high

GABA[b]	2.27	0.866	0.899	marginal	0.851	0.612	marginal
glutamate	2.33	0.664	0.838	marginal	0.647	0.878	marginal
asparagine	2.91	0.818	0.904	marginal	0.707	0.722	marginal
tyrosine	6.90	0.448	0.858	marginal	-	-	-
tryptophan	7.74	0.396	0.982	marginal	0.344	0.793	marginal
β-glucose	5.12	0.656	0.964	marginal	-	-	-
sucrose	5.42	1.448	0.922	high	1.14	0.899	high
allicin	5.54	1.082	0.891	high			-
hydroxycinnamic acids	6.58	0.478	0.911	marginal	0.362	0.860	marginal
$-CH_3$	0.91	1.118	0.879	high	1.135	0.579	moderate
$-CH_2-$	1.33	1.868	0.887	high	2.218	0.611	moderate
$-CH_2-CH=$	2.07	-	-	-	1.269	0.777	high
-CH=CH-	5.34	0.867	0.885	marginal	1.033	0.601	moderate

Sp[c]	**Variable (ppm)**	**VIP**	**p[corr]**	**Significance[e]**	**VIP**	**p[corr]**	**Significance[e]**
leucine	0.97	-	-	-	1.595	-0.766	high
alanine	1.47	-	-	-	1.201	-0.415	moderate
arginine	1.75	-	-	-	1.295	-0.649	moderate
sucrose	5.42	-	-	-	1.150	-0.407	moderate

-C*H*$_3$	0.91	-	-	-	3.026	-0.736	moderate
-C*H*$_2$-	1.33	-	-	-	4.888	-0.652	moderate
-C*H*$_2$ β CO	1.59	-	-	-	1.923	-0.747	high
-C*H*$_2$-CH=	2.07	-	-	-	3.057	-0.755	high
-C*H*$_2$-CH$_2$-CH=	2.27	-	-	-	2.172	-0.736	moderate
=CH-C*H*$_2$-CH=	2.79	-	-	-	2.268	-0.812	high
-C*H*=C*H*-	5.32	-	-	-	2.868	-0.836	high
IE[c]	**Variable (ppm)**	**VIP**	**p[corr]**	**Significance[e]**	**VIP**	**p[corr]**	**Significance[e]**
cycloalliin	1.51	-	-	-	1.592	0.665	moderate
glutamine	2.47	-	-	-	2.162	0.764	high
glutamate	2.36	-	-	-	1.327	0.711	moderate
asparagine	2.89	-	-	-	1.192	0.558	moderate
β-glucose	3.31	-	-	-	1.139	0.516	moderate
fructose	4.05	-	-	-	2.252	0.781	high
threonine	4.27	-	-	-	1.712	0.627	moderate
methanol	3.33	-	-	-	1.436	0.702	moderate
hydroxycinnamic acids	7.66	-	-	-	1.021	0.540	moderate

a) C from HR-MAS model Fig. 3d; Sp+IE from HR-μMAS model Fig. 3f.

b) GABA: γ-aminobutyric acid

c) From the HR-μMAS model Fig. 4b.

d) Errors in chemical shift of ± 0.02 ppm (i.e. bucket increment).

e) High significance (VIP ≥ 1, |p[corr]| ≥ 0.75); moderate significance (VIP ≥ 1, 0.6 ≤ |p[corr]| ≤ ±0.75) except for the Sp vs IE discrimination (0.5 ≤ |p[corr]| ≤ ±0.75); and marginal significance (VIP < 1, |p[corr]| ≥ 0.75).

Table 3. Quantified variant metabolites[a] in µmol/g in Sp and IE: mean ± standard deviation (n=6).

Metabolite	Chemical shift (ppm)[b], No H	Sp	IE	p-value[c]
Alanine	1.39-1.45, 3H	124.5 ± 47.3	-	-
Cycloalliin	1.45-1.51, 3H	67.7 ± 33.2	146.1 ± 31.3	0.00184
Glutamine	2.50-2.41, 2H	476.8 ± 143.1	1016.3 ± 171.3	0.000167
Methanol	3.33-3.30, 3H	-	107.8 ± 28.6	-
Fructose	4.16-4.09, 2H	491.3 ± 93.3	873.1 ± 175.9	0.00177
Sucrose	5.46-5.38, 1H	711.4 ± 121.9	732.8 ± 107.8	0.753
Allicin	6.02-5.86, 1H	546.9 ± 108.9	635.8 ± 207.5	0.381

a) Quantified values are considered estimations.

b) From the acquired HR-µMAS spectra.

c) Student's t-test performed with n = 6, bilateral distribution, different variances.

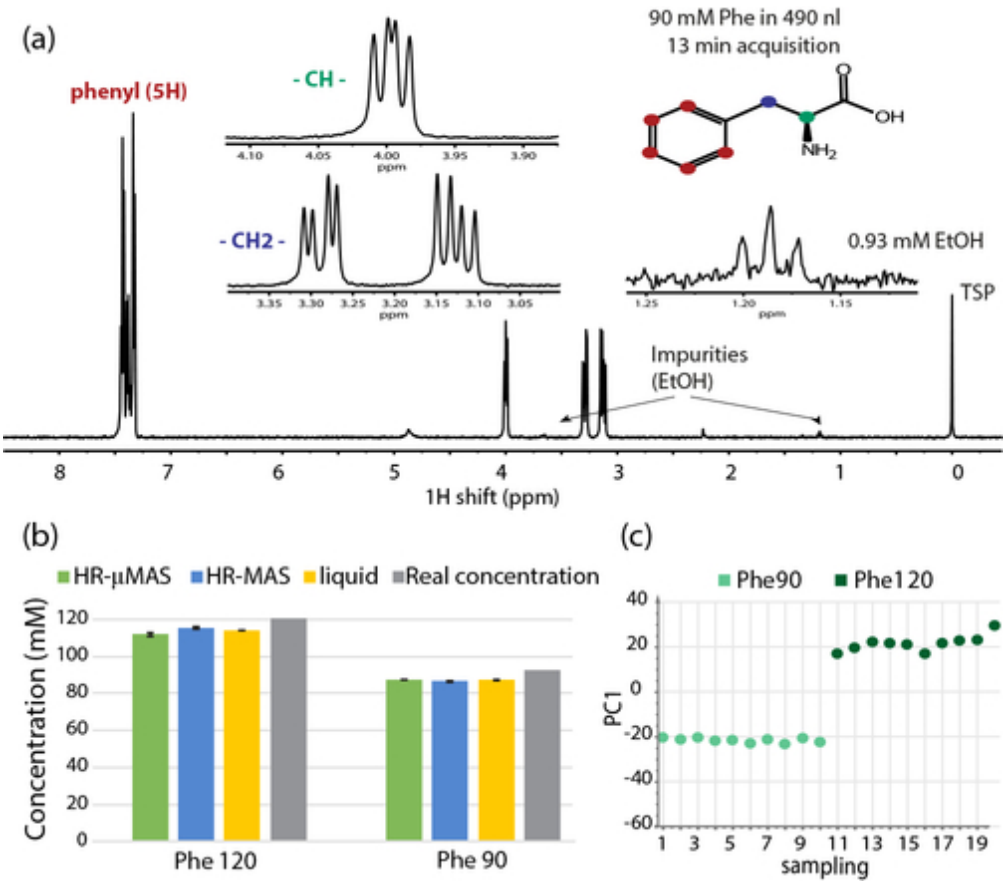

Figure 1 (a) A representative HR-µMAS 1H NMR spectrum of Phe 90 mM (at 500 MHz). The chemical shift ranges between 3.0–3.4 and 3.9–4.1 ppm are expanded for clarity. Signals from the EtOH impurity are highlighted and quantified. (b) A bar plot with the measured concentrations of Phe solutions and their standard deviations of the three different NMR approaches (green = HR-µMAS, blue = HR-MAS, yellow = standard liquid). The expected concentration is plotted for comparative purposes (grey). (c) PCA score plot of acquired NMR data from HR-µMAS. Quality parameters: 1-component, R2X = 0.727, Q2 = 0.69.

42x37mm (300 x 300 DPI)

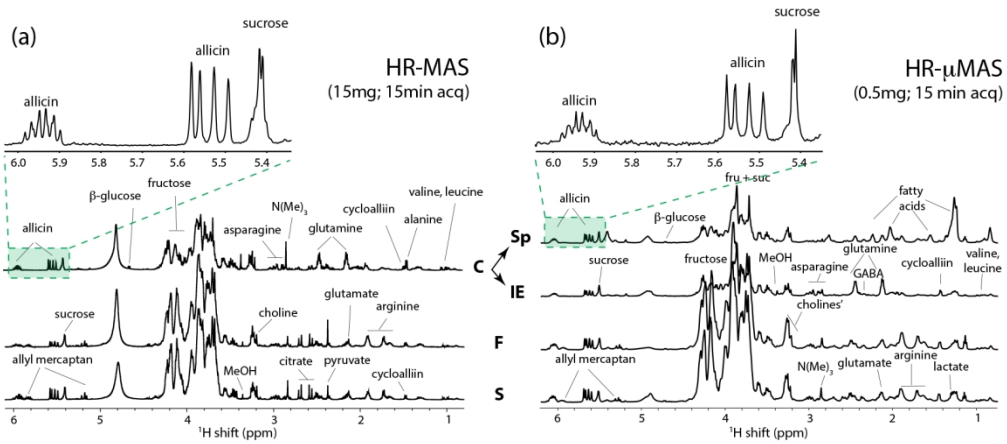

Figure 2 Spectral comparison of the garlic regions between (a) HR-MAS and (b) HR-µMAS. The intensities are normalized to that of the sucrose signal at 5.42 ppm. The assigned metabolites are indicated. The chemical shift range between 5.3–6.0 ppm is amplified showcasing the spectral quality.

153x67mm (300 x 300 DPI)

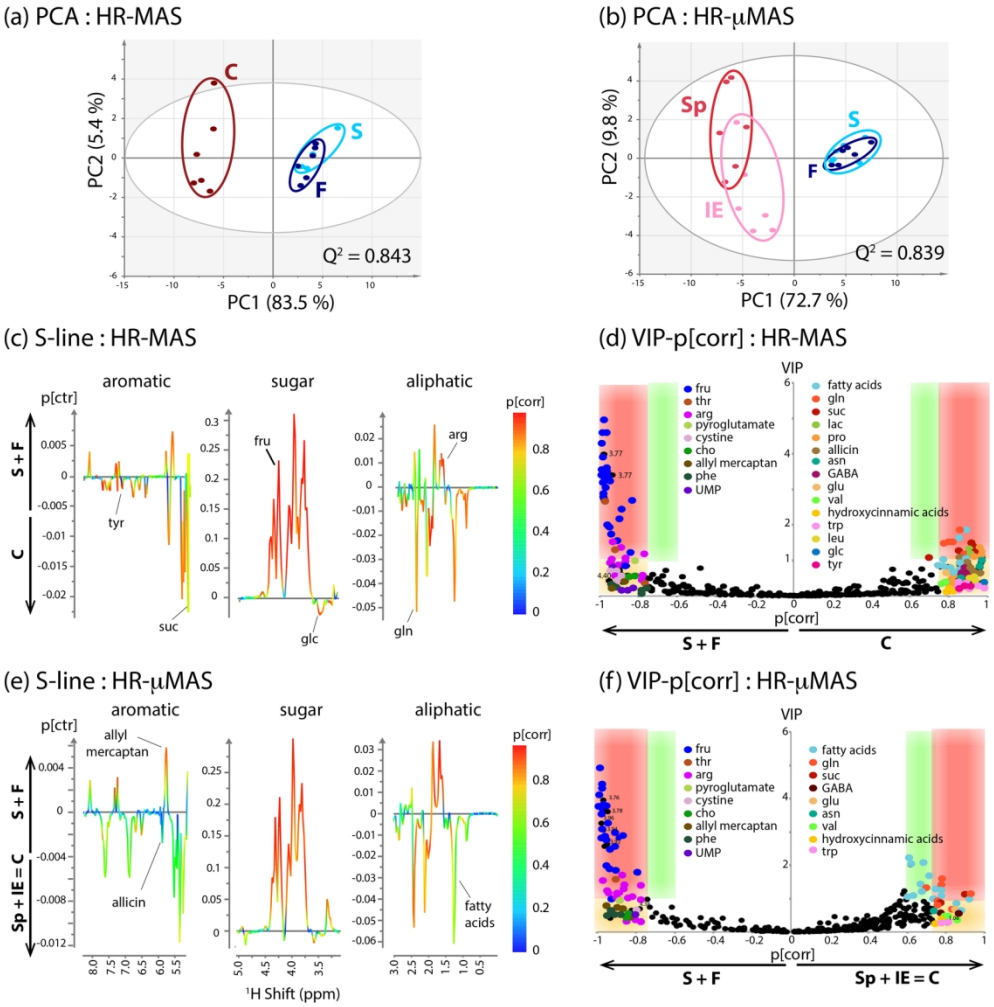

Figure 3 PCA score plots obtained for the separation of the garlic regions using the (a) HR-MAS spectral data and (b) HR-µMAS. The spectra data corresponding to skin (S), flesh (F) and core (C) for HR-MAS; and S, F, sprout (Sp) and inner epidermis (IE) for HR-MAS, are clustered in specific colors for a better readability. Quality parameters: for HR-MAS, 3-components, R2X = 0.919, Q2 = 0.843; for HR-µMAS, 5-components, R2X = 0.934, Q2 = 0.839. The corresponding OPLS-DA were carried out to identify the latent variants. The S-line plots (c) HR-MAS and (e) HR-µMAS identify a few significant variables in S+F (p[ctr] > 0) and C (p[ctr] < 0) in HR-MAS, or Sp+IE (p[ctr] < 0) in HR-µMAS. The significant level p[corr] is indicated by a color scheme. The VIP-p[corr] plots (e) HR-MAS and (f) HR-µMAS facilitate the identification of a complete list of metabolic variants. Quality parameters of OPLS-DA: for HR-MAS, 1 predictive component and 1 orthogonal component, R2X = 0.888, R2Y = 0.982, Q2 = 0.968, p-value (CV) = 7.61*10-9; and for HR-µMAS, 1 predictive component and 1 orthogonal component, R2X = 0.806, R2Y = 0.975, Q2 = 0.964, p-value (CV) = 1.81*10-13.

151x154mm (300 x 300 DPI)

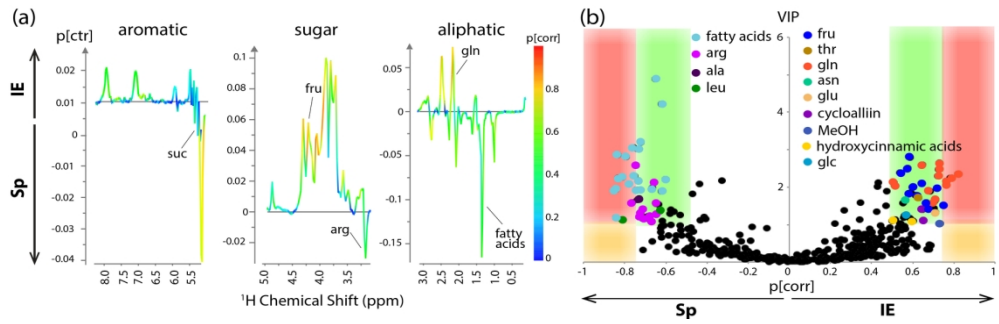

Figure 4 (a) S-line plot and (b) VIP-p[corr] plot used to identify the significant variables responsible of variations between Sp and IE. Quality parameters of OPLS-DA: 1 predictive component and 2 orthogonal components, R2X = 0.747, R2Y = 0.955, Q2 = 0.828, p-value (CV) = 0.027.

161x51mm (300 x 300 DPI)

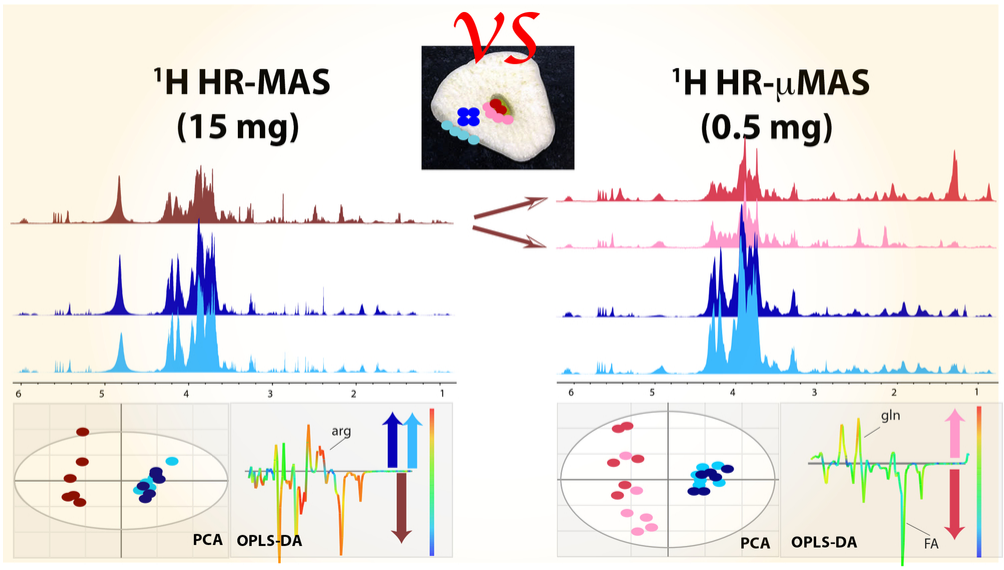

TOC

84x47mm (300 x 300 DPI)